2020 IEEE International Conference on Robotics and Automation (ICRA)
31 May - 31 August, 2020. Paris, France

A Continuum Manipulator with Closed-form Inverse Kinematics and Independently Tunable Stiffness

Bin Zhao, *Student Member, IEEE*, Lingyun Zeng, Baibo Wu and Kai Xu, *Member, IEEE*

***Abstract*— Continuum manipulators can accomplish various tasks in confined spaces, benefiting from their compliant structures and improved dexterity. Confined and unstructured spaces may require both enhanced stiffness of a continuum manipulator for precision and payload, as well as compliance for safe interaction. Thus, studies have been consistently dedicated to design continuum or articulated manipulators with tunable stiffness to adapt to different operating conditions. This paper presents a continuum manipulator with independently tunable stiffness where the stiffness variation does not affect the movement of the manipulator's end-effector. Moreover, the proposed continuum manipulator is found to have analytical inverse kinematics. The design concept, analytical kinematics, system construction and experimental characterizations are presented. The results showed that the manipulator's stiffness can be increased up to 3.61 times of the minimal value, demonstrating the effectiveness of the proposed idea.**

I. Introduction

Continuum manipulators have been of interest due to their improved dexterity in confined spaces and intrinsic compliant interaction in unstructured spaces. For example, slender continuum manipulators have been applied in surgical robots [1] and field operations [2, 3]. The continuum manipulator with tunable stiffness is desired to adapt to different operating conditions. Enhanced stiffness of a continuum manipulator is desired for precision and payload, while the compliance is preferred for safe interaction, preventing possible damages to fragile nearby objects or structures.

Hence, recent researches have focused on exploring possible designs for manipulators with tunable stiffness. For example, active materials can be used as tunable stiffness elements, including magnetorheological fluids [4], electrorheological fluids [5] or thermally softened alloy or plastics [6, 7]. However, the uses of active materials usually complicate the robotic system. In addition, the response can be slow for thermally activated materials (on the order of seconds).

Tunable stiffness can also be achieved by controlling the friction between the structural elements. For example, in tendon-driven manipulators, high tension forces from the pulling wires compress the vertebrae such that higher friction is generated from the contacting surfaces [8-12]. On the other hand, jamming can be used to introduce higher friction via pressurization for tunable stiffness [13-16]. However, the friction-based stiffness enhancement often leads to actuation hysteresis.

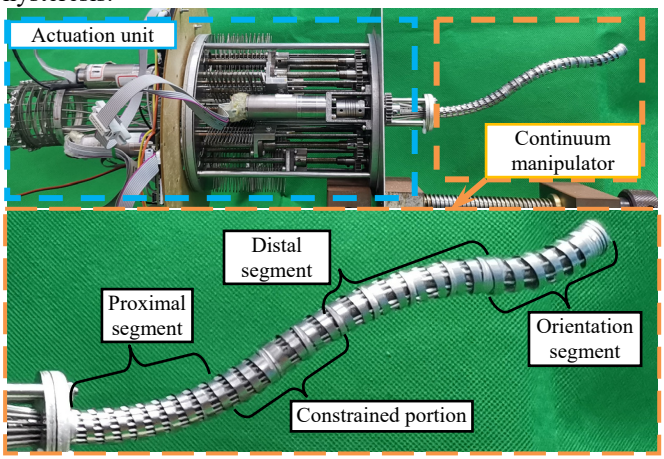

Fig. 1. The constructed continuum manipulator with closed-form inverse kinematics and independently tunable stiffness

It is possible to achieve tunable stiffness via proper controller design. For example, a modified position controller drove a concentric-tube manipulator into different poses for different stiffness upon understanding its mechanics [17]. A stiffness controller utilized the manipulator's intrinsic force sensing capability that was proposed in [18] to realize variable stiffness [19]. The controller-based approaches can be challenging in formulating the stiffness model based on the manipulator's mechanics.

Furthermore, stiffness can be enhanced via structure variations, such as the inclusion of a motion constraining kinematic chain [20]. However, such approach often complicated the system construction.

This paper hence proposes a continuum manipulator design with independently tunable stiffness. The manipulator with its actuation unit is shown in Fig. 1. As detailed in Section II, the manipulator's stiffness can be continuously tuned by moving a rigid tube inside the manipulator such that the constrained portion can be at different positions along the manipulator. It was found that the changed positions of the constrained portion will not change the position and orientation of the orientation segment, even though the manipulator's shape is indeed changed. This is hence referred to as independently

*This work was supported in part by the National Natural Science Foundation of China (Grant No. 51722507, Grant No. 51435010 and Grant No. 91648103), and in part by the National Key R&D Program of China (Grant No. 2017YFC0110800).

Bin Zhao is with the RII Lab (Lab of Robotics Innovation and Intervention), UM-SJTU Joint Institute, Shanghai Jiao Tong University, Shanghai, China (emails: zhaobin2014@sjtu.edu.cn)

Lingyun Zeng, Baibo Wu and Kai Xu are with School of Mechanical Engineering, Shanghai Jiao Tong University, Shanghai, China (emails: me_maxqi@sjtu.edu.cn, wubaibo@sjtu.edu.cn, and k.xu@sjtu.edu.cn ; corresponding author: Kai Xu).

tunable stiffness with respect to the movement of the manipulator's end-effector.

The stiffness variation approach in the proposed design is similar to the authors' previous work [21]. However, the stiffness variation is associated with the position and orientation changes of the end effector in [21]. Namely, the stiffness is not independently tunable. On the other hand, the proposed idea of changing the position of a rigid structural component is similar to the insertion of the equilibrium modulation backbone in [22]. But the equilibrium modulation backbone is inserted for generating fine position outputs, other than varying stiffness.

Moreover, the proposed manipulator is found to have closed-form inverse kinematics. Kinematics modeling of continuum robots often relies on a circular shape assumption of the segments [23]. And the inverse kinematics can be solved numerically [24-26] or iteration-based heuristically [27]. Closed-form inverse kinematic solutions for extensible bending segments were proposed in [28] and [29]. But the aforementioned two methods cannot be applied to continuum robots with inextensible bending segments. The proposed inverse kinematics here is for inextensible bending segments under the proposed specific segment arrangement.

Contributions of this work hence lie on the proposed design with i) independently tunable stiffness, and ii) analytical inverse kinematics formulation. System construction and experimental characterizations are presented to demonstrate the effectiveness of the proposed idea.

This paper is organized as follows. Section II explains the design concept. Section III presents the closed-form kinematics. The prototype design and construction are described in Section IV. The experimental characterizations for verifying the independently tunable stiffness are presented in Section V, with the conclusions summarized in Section VI.

II. Design Concept

This study proposes a continuum manipulator design with independently tunable stiffness. The continuum manipulator consists of an inverted dual continuum mechanism (IDCM) and an orientation segment, as shown in Fig. 2(a). The IDCM can generate translations of the orientation segment, while the orientation segment orients the continuum manipulator tip.

In this design, the IDCM consists of a proximal segment (PS), a distal segment (DS), a constrained portion and an actuation segment (AS). The PS and the DS are structurally identical. Each segment consists of a few super-elastic nitinol structural backbones, an end disk and several spacer disks. The structural backbones are attached to the end disks of the DS and the PS, and the spacer disks prevent buckling of the structural backbones. Since the total lengths of the structural backbones remain constant, the identical bending of the PS and DS would be generated in the opposite direction. Thus, the DS's end disk would be always parallel to that of the PS. The IDCM could seem similar to flexure parallelograms. But the IDCM generates 2-DoF (Degree of Freedom) motions, while flexure parallelograms often only generate planar motions.

An AS, which is structurally similar to the DS or PS, is integrated to bend the PS. As shown in Fig. 2, the AS is bent by actuating its actuation backbones. Then the PS and DS are bent, and pure translations of the IDCM are hence generated.

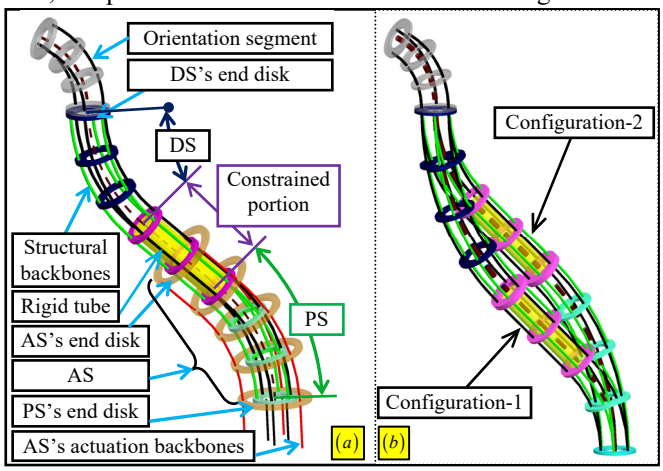

Fig. 2. Design concept: a) the continuum manipulator consists of an IDCM with a constrained portion, and an orientation segment, and b) stiffness variation is achieved via altering the constrained portion's position.

The IDCM is inspired from the dual continuum mechanism proposed in [30] where the base disks of the DS and PS are grounded. The IDCM is created by grounding PS's end disk.

The actuation backbones in the IDCM's AS and the orientation segment are actuated by the actuation unit, as explained in the Section IV.

The proposed stiffness tuning is achieved as a straight rigid tube is inserted inside of the IDCM to constrain the bending of the PS and the DS, as shown in Fig. 2(a). The position of the constrained portion along the IDCM can be determined by the length of the PS, l_p. As shown in the kinematics model in Section III, it is found that the tip positions of the IDCM are not affected by the position of the constrained portion, as shown in Fig. 2(b). A shorter PS may lead to higher stiffness. This is hence referred to as independently tunable stiffness with respect to the IDCM's tip position, even though the IDCM's shape is indeed changed.

What's more, it was further found that the proposed continuum manipulator has analytical inverse kinematics, which is detailed in Section III.C.

The IDCM was used in a previous work for designing a surgical manipulator [31]. But it is in this paper that the IDCM with the constrained portion is proposed to achieve independently tunable stiffness and the analytical inverse kinematics is derived.

III. Kinematics

The nomenclature and the coordinates are presented in Section III.A. The kinematics of a single continuum segment, the IDCM, and the continuum manipulator are derived in Section III.B, Section III.C, and Section IV.D, respectively.

A. Nomenclature and Modeling Assumptions

The nomenclature and the coordinates are defined for the proposed continuum manipulator, as in Table I and Fig. 3. For

visualization clarity, only three backbones for each segment are shown in the Fig. 2 and Fig. 3. The number of backbones in the prototype is different.

TABLE I
NOMENCLATURE USED IN THE KINEMATICS MODEL

Symbol	Definition
i	Index of the continuum segments. $i = p$, d and o. The index p means the proximal segment, while d stands for the distal segment and o stands for the orientation segment.
l_i	l_p, l_d and l_o refer to the lengths of the PS, DS, and orientation segment, measured along the virtual central backbone.
l_r	The length of the constrained portion.
l_{total}	$l_{total} = l_p + l_d + l_r + l_o$
θ_i	Bending angle of the continuum segment
δ_i	Rotation angle from $\hat{\mathbf{y}}_{i1}$ to $\hat{\mathbf{x}}_{ib}$ along $\hat{\mathbf{z}}_{ib}$.
$\boldsymbol{\psi}_p$	Configuration vectors of the IDCM: $\boldsymbol{\psi}_p = [\theta_p \; \delta_p]^T$
$\boldsymbol{\psi}_o$	Configuration vector of the orientation segment. $\boldsymbol{\psi}_o = [\theta_o \; \delta_o]^T$
$\boldsymbol{\psi}$	Configuration vector of continuum manipulator. $\boldsymbol{\psi} = [\boldsymbol{\psi}_p^T \; \boldsymbol{\psi}_o^T]^T$
c_θ, s_θ	$\cos(\theta)$, $\sin(\theta)$

- Base Disk Coordinate $\{ib\} \equiv \{\hat{\mathbf{x}}_{ib}, \hat{\mathbf{y}}_{ib}, \hat{\mathbf{z}}_{ib}\}$ is attached to the segment's base disk with its origin at the disk's center. $\hat{\mathbf{x}}_{ib}$ points from the center to the first backbone.
- Bending Plane Coordinate-1 $\{i1\} \equiv \{\hat{\mathbf{x}}_{i1}, \hat{\mathbf{y}}_{i1}, \hat{\mathbf{z}}_{i1}\}$ shares origin with $\{ib\}$ and has the continuum segment bent in its XY plane.

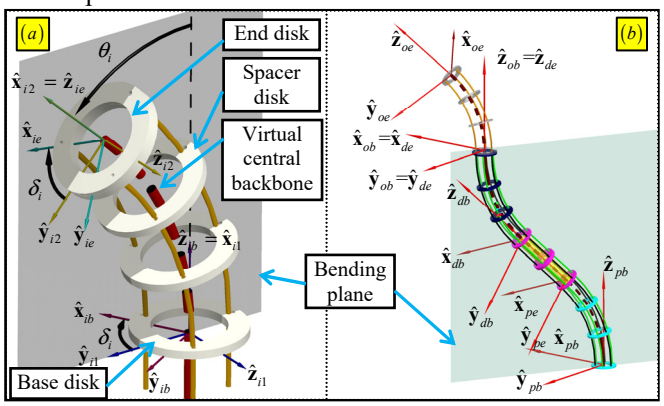

Fig. 3. Coordinates attachement and nomenclature of (a) the single continuum segment, and (b) the continuum manipulator.

- Bending Plane Coordinate-2 $\{i2\} \equiv \{\hat{\mathbf{x}}_{i2}, \hat{\mathbf{y}}_{i2}, \hat{\mathbf{z}}_{i2}\}$ is obtained from $\{i1\}$ by a rotation about $\hat{\mathbf{z}}_{i1}$ such that $\hat{\mathbf{x}}_{i2}$ becomes the virtual central backbone tangent at the end disk.
- End Disk Coordinate $\{ie\} \equiv \{\hat{\mathbf{x}}_{ie}, \hat{\mathbf{y}}_{ie}, \hat{\mathbf{z}}_{ie}\}$ is attached to the end disk. $\hat{\mathbf{x}}_{ie}$ points from the center to the first backbone, and $\hat{\mathbf{z}}_{ie}$ is normal to the end disk.

Two modeling assumptions are used.

- A virtual central backbone characterizes the length and shape of the continuum segment. The kinematics assumes a circular shape for the segments, referring to [32].
- The position of the constrained portion along the virtual central backbone is determined by the length of the PS, l_p. The lengths of the PS and the DS can be continuously changed via the insertion of the rigid tube.

B. Kinematics of a single continuum segment

The continuum segments, including the DS, the PS and the orientation segment, are inextensible with two bending DoFs, specified by the configuration vector $\boldsymbol{\psi}_i \equiv [\theta_i \; \delta_i]^T$. The length is l_i. The position of $\{ie\}$ in $\{ib\}$, ${}^{ib}\mathbf{p}_{ie}$, is written as in (1).

$$ {}^{ib}\mathbf{p}_{ie} = (l_i/\theta_i)\begin{bmatrix} c_{\delta_i}(1-c_{\theta_i}) & s_{\delta_i}(c_{\theta_i}-1) & s_{\theta_i} \end{bmatrix}^T \tag{1} $$

Where ${}^{ib}\mathbf{p}_{ie} = [0 \; 0 \; l_i]^T$, when $\theta_i = 0$.

The orientation of $\{ie\}$ in $\{ib\}$ is written as in (2), referring to the previous study [26].

$$ {}^{ib}\mathbf{R}_{ie} = \begin{bmatrix} c_{\theta_i}(c_{\delta_i})^2 + (s_{\delta_i})^2 & s_{\delta_i} c_{\delta_i}(1-c_{\theta_i}) & c_{\delta_i} s_{\theta_i} \\ s_{\delta_i} c_{\delta_i}(1-c_{\theta_i}) & c_{\theta_i}(s_{\delta_i})^2 + (c_{\delta_i})^2 & -s_{\delta_i} s_{\theta_i} \\ -c_{\delta_i} s_{\theta_i} & s_{\delta_i} s_{\theta_i} & c_{\theta_i} \end{bmatrix} \tag{2} $$

The inverse kinematics of a single continuum segment can be derived as follows to obtain the configuration vector $\boldsymbol{\psi}_i$ from a given orientation ${}^{ib}\mathbf{R}_{ie}$.

$$ \begin{aligned} \theta_i &= \text{acos}({}^{ib}\mathbf{R}_{ie,33}) \\ \delta_i &= \text{atan2}(-{}^{ib}\mathbf{R}_{ie,23}, {}^{ib}\mathbf{R}_{ie,13}) \end{aligned} \tag{3} $$

Where the function atan2 gives the angle between the positive x-axis and the ray passing the point $(-{}^{ib}\mathbf{R}_{ie,23}, {}^{ib}\mathbf{R}_{ie,13}) \neq (0,0)$. It should be noted that the use of the function atan2 can eliminate the algorithmic singularity introduced by an arctan function.

C. Kinematics of the IDCM

Translational movements of the IDCM would be generated due to the identical bending of the DS and the PS. Hence, configuration of the IDCM is specified by the configuration vector of the PS $\boldsymbol{\psi}_p \equiv [\theta_p \; \delta_p]^T$. The IDCM's shape can be described by a path in the bending plane sequentially along:

- The virtual central backbone of the PS (a circular arc of length l_p and bending angle θ_p), and the position ${}^{pb}\mathbf{p}_{pe}$ and orientation ${}^{pb}\mathbf{R}_{pe}$ can be calculated referring to (1) and (2);
- The axis of constrained potion with a distance of l_r, hence, the $\{db\}$ is located in $\{pe\}$ at ${}^{pe}\mathbf{p}_{db} = [0 \; 0 \; l_r]^T$; and
- The virtual central backbone of the DS (a circular arc of length l_d and bending angle $\theta_d = \theta_p$), and the tip position ${}^{db}\mathbf{p}_{de}$ also can be obtained according to (1).

As the bending plane is represented by δ_p, the expression of ${}^{pb}\mathbf{p}_{de}$ is hence derived as in (4).

$$ \begin{aligned} {}^{pb}\mathbf{p}_{de} &= {}^{pb}\mathbf{p}_{pe} + {}^{pb}\mathbf{R}_{pe}({}^{pe}\mathbf{p}_{db} + {}^{db}\mathbf{p}_{de}) \\ &= \begin{bmatrix} c_{\delta_p}\left((1-c_{\theta_p})(l_p+l_d)/\theta_p + l_r s_{\theta_p}\right) \\ -s_{\delta_p}\left((1-c_{\theta_p})(l_p+l_d)/\theta_p + l_r s_{\theta_p}\right) \\ s_{\theta_p}(l_p+l_d)/\theta_p + l_r c_{\theta_p} \end{bmatrix} \end{aligned} \tag{4} $$

Where ${}^{pb}\mathbf{p}_{de} = [0 \; 0 \; l_p + l_d + l_r]^T$, when $\theta_p = 0$.

Let $l_b = l_p + l_d$ is the total length of the PS and DS. The l_b is constant in the design, regardless of the changes of l_p.

Since the tip movement of the IDCM is purely translational, the orientation of $\{de\}$ w.r.t $\{pb\}$, ${}^{pb}\mathbf{R}_{de}$, is an identity matrix.

$$ {}^{pb}\mathbf{R}_{de} = \mathbf{I}_{3\times 3} \tag{5} $$

It's worth noting that the location of the rigid tube, l_p, does not affect the position ${}^{db}\mathbf{p}_{de}$ and the orientation ${}^{pb}\mathbf{R}_{de}$. Referring to (4), l_p alone does not change the value of ${}^{db}\mathbf{p}_{de}$. As long as $l_b = l_p + l_d$ is constant, altering the position of the constrained portion could be used to achieve the stiffness variation without affecting the movements of the continuum manipulator.

The closed-form inverse kinematics of the IDCM can be derived as follows.

The orientation of the end effector of the continuum manipulator is determined by the orientation segment, since the IDCM only provides translations. Then, when the desired pose of the continuum manipulator is given, the configuration of the orientation segment can be obtained from the desired orientation. Next, tip position of the IDCM can be calculated from the determined shape of the orientation segment.

Observing (4), it can be seen that δ_p, from the configuration vector $\boldsymbol{\psi}_p \equiv [\theta_p \ \delta_p]^T$, can be easily obtained as in (6).

$$\delta_p = \operatorname{atan2}(-{}^{pb}\mathbf{p}_{de}\big|_y, {}^{pb}\mathbf{p}_{de}\big|_x) \tag{6}$$

Then, δ_p can be eliminated as in (7).

$$r_s = +\sqrt{{}^{pb}\mathbf{p}_{de|x}^2 + {}^{pb}\mathbf{p}_{de|y}^2} = (1-\mathrm{c}_{\theta_p}) l_b/\theta_p + l_r \mathrm{s}_{\theta_p} \tag{7}$$

It was found that the θ_p term can be further eliminated as in (8). Next, the half angle formulas can be used to generate (10).

$$\frac{r_s - l_r \mathrm{s}_{\theta_p}}{{}^{pb}\mathbf{p}_{de}\big|_z - l_r \mathrm{c}_{\theta_p}} = \frac{(1-\mathrm{c}_{\theta_p})\frac{l_b}{\theta_p}}{\mathrm{s}_{\theta_p}\frac{l_b}{\theta_p}} = \frac{(1-\mathrm{c}_{\theta_p})}{\mathrm{s}_{\theta_p}} \tag{8}$$

Equation (8) leads to (9).

$$\begin{aligned} &\left(r_s - l_r \mathrm{s}_{\theta_p}\right)\mathrm{s}_{\theta_p} = \left({}^{pb}\mathbf{p}_{de}\big|_z - l_r \mathrm{c}_{\theta_p}\right)(1-\mathrm{c}_{\theta_p}) \\ &\Rightarrow r_s \mathrm{s}_{\theta_p} - l_r \mathrm{s}_{\theta_p}^2 = {}^{pb}\mathbf{p}_{de}\big|_z - l_r \mathrm{c}_{\theta_p} - \mathrm{c}_{\theta_p}\,{}^{pb}\mathbf{p}_{de}\big|_z + l_r \mathrm{c}_{\theta_p}^2 \\ &\Rightarrow r_s \mathrm{s}_{\theta_p} = \left({}^{pb}\mathbf{p}_{de}\big|_z + l_r\right)\left(1-\mathrm{c}_{\theta_p}\right) \end{aligned} \tag{9}$$

Then, Equation (10) can be obtained by substituting the half angle formulas of $\sin\theta_p = 2\sin(\theta_p/2)\cos(\theta_p/2)$ and $\cos\theta_p = 1 - 2\sin^2(\theta_p/2)$. θ_p is hence obtained as in (11).

$$\tan(\theta_p/2) = r_s \Big/ \left({}^{pb}\mathbf{p}_{de}\big|_z + l_r\right) \tag{10}$$

$$\theta_p = 2 \cdot \operatorname{atan2}(r_s, {}^{pb}\mathbf{p}_{de}\big|_z + l_r) \tag{11}$$

D. Kinematics of the continuum manipulator

The orientation segment is stacked on top of the IDCM to form the proposed continuum manipulator. $\{ob\}$ coincides with $\{de\}$. Hence, the tip position ${}^{pb}\mathbf{p}_{oe}$ of the continuum manipulator can be calculated as follows.

$${}^{pb}\mathbf{p}_{oe} = {}^{pb}\mathbf{p}_{de} + {}^{pb}\mathbf{R}_{de}\,{}^{ob}\mathbf{p}_{oe} = {}^{pb}\mathbf{p}_{de} + {}^{ob}\mathbf{p}_{oe} \tag{12}$$

The orientation ${}^{pb}\mathbf{R}_{oe}$ of $\{oe\}$ in $\{pb\}$ is obtained as follows.

$${}^{pb}\mathbf{R}_{oe} = {}^{pb}\mathbf{R}_{de}\,{}^{ob}\mathbf{R}_{oe} = {}^{ob}\mathbf{R}_{oe} \tag{13}$$

The closed-form inverse kinematics of the proposed continuum manipulator is derived as follows.

Firstly, the configuration vector of the orientation segment, $\boldsymbol{\psi}_o$, is obtained as in (3), since the orientation of the proposed continuum manipulator only depend on the orientation segment. Then, tip position of the IDCM, ${}^{pb}\mathbf{p}_{de}$, is calculated from ${}^{pb}\mathbf{p}_{oe}$ and $\boldsymbol{\psi}_o$ as in (14).

$${}^{pb}\mathbf{p}_{de} = {}^{pb}\mathbf{p}_{oe} - {}^{ob}\mathbf{p}_{oe} \tag{14}$$

Finally, the configuration vector $\boldsymbol{\psi}_p$ of the IDCM can be calculated according to (6) and (11) with ${}^{pb}\mathbf{p}_{de}$ obtained from (14). The closed-form inverse kinematics is fully obtained.

The parameters of the manipulator are listed in TABLE II.

TABLE II
PARAMETERS OF THE CONTINUUM MANIPULATOR

l_b = 110 mm	l_r = 50mm	l_o = 35mm	$l_p \in$ [30mm, 80mm]
$\theta_p \in [0°,90°]$	$\delta_p \in (-180°,180°]$	$\theta_o \in [0°,90°]$	$\delta_o \in (-180°,180°]$

IV. Design Description

The continuum manipulator shown in Fig. 4 with closed-form inverse kinematics and independently tunable stiffness is driven by an actuation unit shown in Fig. 5. The actuation unit alters the position of the constrained portion as well. The control infrastructure is also briefly introduced.

A. Continuum Manipulator

The schematic of the continuum manipulator which is formed by serially connecting the IDCM and the orientation segment is shown in Fig. 4(b).

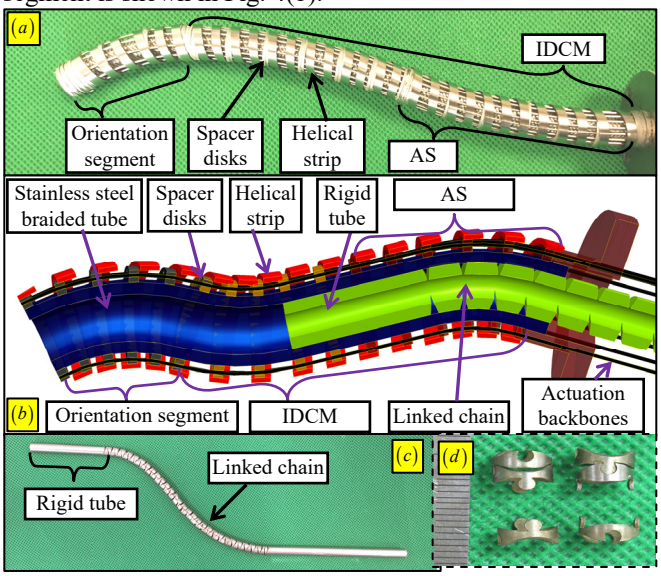

Fig. 4. Design details: (a) the continuum manipulator without the constrained portion, (b) the schematic, (c) the linked chain, and (d) the links

In this specific IDCM design, the AS from Section II is merged with the PS. The IDCM possesses four structural nitinol backbones, and its AS is bent by actuating four actuation backbones. These backbones all have diameter of 0.7mm. The orientation segment has eight structural backbones. As shown in Fig. 4(a), a stainless steel helical strip with the wall thickness of 0.1 mm was utilized to separate the spacer disks. A stainless steel braided tube is attached inside the spacer disks. It is flexible enough to be bent and it provides a smooth and continuous surface for inserting the stainless steel rigid tube to constrain the PS and DS. The rigid tube has an outer diameter of 7mm and an inner diameter of 6 mm.

An important enabling mechanism is to allow the translation of the rigid tube inside the IDCM without affecting bending the PS of the IDCM. Here a linked chain was designed as shown in Fig. 4(c). The linked chain is composed of articulated links that are cut from a tube, as shown in Fig. 4(d). The linked chain has high axial rigidity for transmitting pushing and pulling, while it has near-zero bending stiffness such that bending of the continuum segment is not affected.

The linked chain is connected with the stainless steel rigid tube so that the actuation unit translates the linked chain to push or pull the rigid tube as shown in Fig. 5.

B. Actuation Unit

The actuation unit in Fig. 5 is designed to actuate the continuum manipulator as well as alter the position of the constrained portion to vary the stiffness.

An Orientation Proximal Segment (OPS) is integrated to bend the orientation segment. The OPS and the orientation segment formed a dual continuum mechanism, as proposed in [30]. In the design, the OPS is bent by pushing or pulling four actuation backbones simultaneously. The backbones are arranged 90° apart and are attached to the end disk of the OPS.

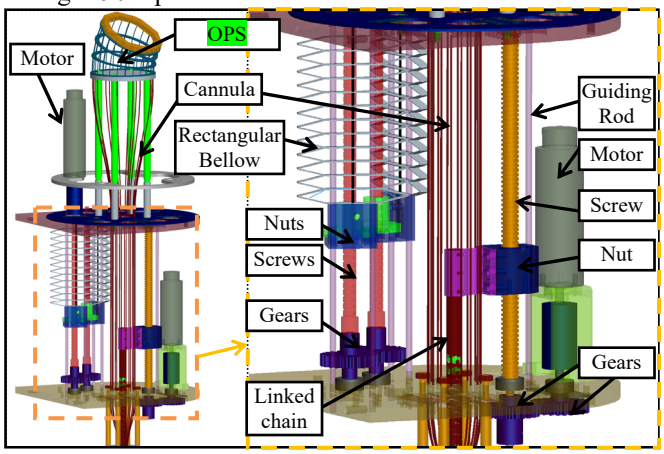

Fig. 5. Schematic of the actuation unit

To push and pull the actuation backbones in the OPS and the AS of the IDCM, four pairs of lead screws were used (two pairs for driving the IDCM's AS and two pairs for driving the OPS). Each pair of the lead screws is coupled via a meshing pair of spur gears, in order to make the nuts simultaneously and equally move in the opposite directions. The actuation backbones are fixed to the nuts, routed through rectangular bellow and a few cannulae. The rectangular bellow can slide on the guiding rods and prevent buckling of the backbones.

The rigid tube is pushed and pulled by the linked chain that is actuated by a motorized lead screw, as shown in Fig. 5.

Five Maxon DCX22L motors were integrated to actuate the screws (two for driving OPS, two for driving the IDCM's AS, and one for changing the position of the constrained portion), while five Maxon EPOS2 24/2 digital controllers were used to drive and control the motors. The desired positions of the motors are calculated in a desktop computer according to the kinematics and transmitted to the digital controllers via a CAN (Controller Area Network) bus.

V. Experimental Characterizations

In order to verify the proposed design concept, numerical simulations and experimental validations were carried out. The simulation of the inverse kinematics is presented in Section V.A. The verification of independently tunable stiffness is presented in Section V.B.

A. Simulation of the Inverse Kinematics

The inverse kinematics of the continuum manipulator in different cases is simulated to show its motions.

In the first case, the end disk of the continuum manipulator is commanded to move on a given plane defined as in (15) and (16), as shown in Fig. 6. It's desired that its end disk of the orientation segment coincides with the given plane.

$$({}^{pb}\mathbf{p}_{oe} - \mathbf{p}_0) \times \mathbf{n} = 0 \tag{15}$$

$${}^{pb}\mathbf{R}_{oe}\mathbf{e}_3 = \mathbf{n} \tag{16}$$

Where $\mathbf{e}_3 = [0\ 0\ 1]^T$ and $\mathbf{n} = [0.577\ 0.577\ 0.577]^T$ is a normal vector that is perpendicular to the desired plane, and $\mathbf{p}_0 = [50.6$ mm 50.6 mm 50.6 mm$]^T$ is a point located in the plane.

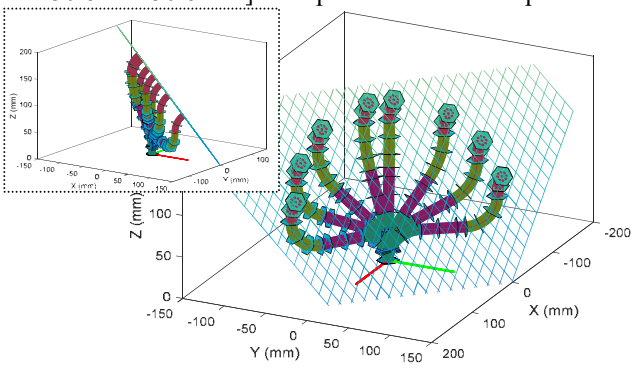

Fig. 6. Simulation of the continuum manipulator configurations corresponding to the manipulator's movements on the given plane

Since the normal vector $\mathbf{n}$ is given, the configuration vector $\boldsymbol{\psi}_o$ of the orientation segment can be obtained according to (3). Then the feasible $\boldsymbol{\psi}_p$ values were obtained via iterating θ_p and solving the corresponding δ_p to check whether (15) holds.

The second case is a motion planning in the configuration space. When the target pose $({}^{pb}\mathbf{p}_{oe}^{tgt}$ and ${}^{pb}\mathbf{R}_{oe}^{tgt})$ is given, its corresponding configuration vector $\boldsymbol{\psi}^{tgt}$ can be calculated according to the closed-form inverse kinematics in Section III.

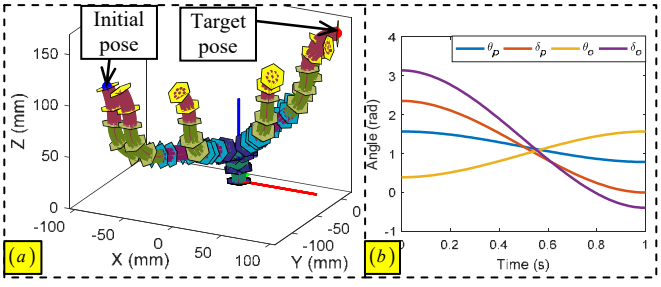

Fig. 7. Simulation of the motion planning in the configuration space: (a) intermediate poses, (b) trajectories of the configuration vector $\boldsymbol{\psi}$

The planning algorithm acts on the configuration vector and satisfies the following boundary conditions:

$$\boldsymbol{\psi}(t_0)=\boldsymbol{\psi}^{cur};\ \dot{\boldsymbol{\psi}}(t_0)=\mathbf{0};\ \boldsymbol{\psi}(t_f)=\boldsymbol{\psi}^{tgt};\ \dot{\boldsymbol{\psi}}(t_f)=\mathbf{0} \quad (17)$$

Where $t_0 = 0$ s is the start time, while $t_f = 1$ s is the end time.

Then a third order polynomial is applied to generate the trajectories of the configuration vector according to (18).

$$\begin{aligned}\boldsymbol{\psi}(t) &= \mathbf{a}_3 t^3 + \mathbf{a}_2 t^2 + \mathbf{a}_1 t + \mathbf{a}_0 \\ \dot{\boldsymbol{\psi}}(t) &= 3\mathbf{a}_3 t^2 + 2\mathbf{a}_2 t + \mathbf{a}_1\end{aligned} \quad (18)$$

Simulation of the continuum manipulator configurations with intervals of 0.2 s is plotted in Fig. 7(a). And the trajectories of the configuration vector are shown in Fig. 7(b).

B. *Verification of the Independently Tunable Stiffness*

Stiffness of the continuum manipulator was quantified under different configurations to demonstrate the effectiveness of the proposed stiffness variation approach.

Firstly, the continuum manipulator was driven to a desired configuration. Then, the position of the constrained portion l_p would be changed to alter the stiffness, as shown in Fig. 8(a). The orientation segment would be kept straight in the study.

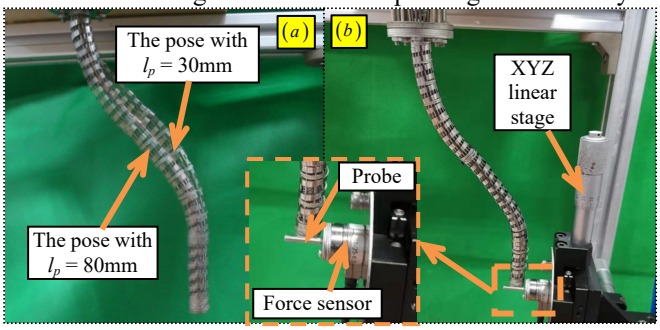

Fig. 8. Verification of tunable stiffness: a) overlaped image of the continuum robots with different positions of constrained portion, and b) experimental setup of stiffness quantification

A 6-axis force sensor (Nano-17, ATI Industrial Automation) with a probe was utilized to measure the exerted force. As shown in Fig. 8(b), the probe on the force sensor was driven by the XYZ linear stage to touch the continuum manipulator's tip, and then move its tip in the X, Y and Z directions in the $\{pb\}$ respectively. For every 0.5 mm perturbation, the exerted forces were measured and recorded, and the total perturbation was 3 mm. The slope between the measured forces and the given movements can be fitted to estimate the stiffness.

The tunable stiffness was verified under three configurations as shown in Fig. 9(a). The stiffness results with respect to the different positions of the constrained portion are plotted in Fig. 9(b), ranging from 30 mm to 80 mm with intervals of 10 mm. A few observations can be made.

- As shown in Fig. 8(a), changing the position of the constrained portion would slightly perturb the orientation segment. The perturbation may results from the friction between the disks and backbones, and the spacing between the rigid tube and the stainless steel braided tube.
- It can be seen that the continuum manipulator with a shorter proximal segment possesses higher stiffness.
- Changing the position of the constrained portion of the IDCM can effectively adjust the tip stiffness of continuum manipulator. The stiffness is increased from 1.34 times in the X-direction of Config-2 to 3.61 times in the Y-direction of Config-3 of the minimal values.

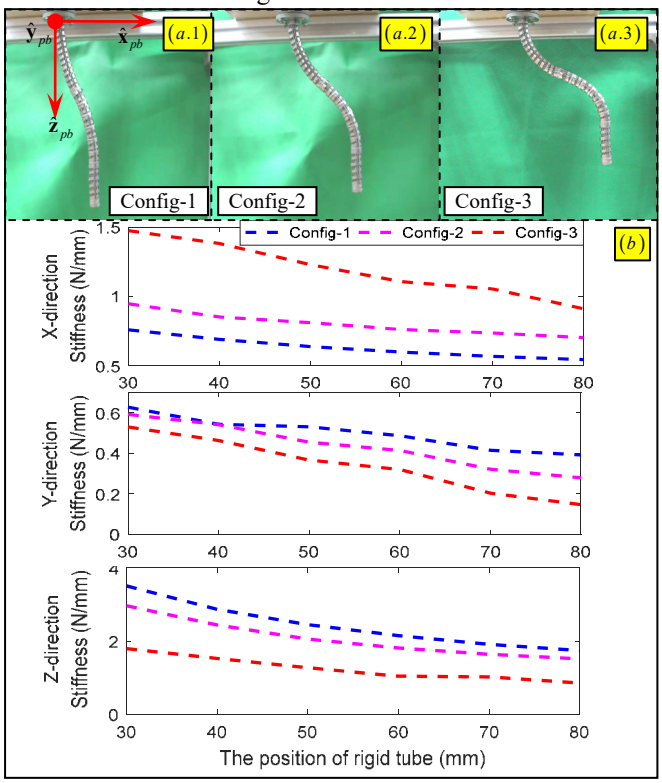

Fig. 9. Stiffness characterizations: a) poses under three configurations: (a.1) Config-1, (a.2) Config-2, and (a.3) Config-3; b) the stiffness results in the X, Y and Z directions with respect to different l_p lengths (a.k.a, positions of the constrained portion) from 30mm to 80mm

VI. Conclusion

Continuum manipulators have become popular in various applications in confined spaces because of their inherently safe interactions and distal dexterity. They are at times expected to have tunable stiffness to handle different tasks. For example, in surgical applications, high stiffness can be used for accurate tissue dissection and suture penetration, while low stiffness can be used for tissue separation to prevent damaging the tissue.

The paper proposes a continuum manipulator with closed-form inverse kinematics and independently tunable stiffness. An inverted dual continuum mechanism is proposed with a constrained portion. The independently tunable stiffness is achieved by altering the position of the constrained portion without affecting the tip pose of the continuum manipulator. The design concept, system construction, closed-form kinematics and experimental validations are detailed. Experimental results show that the continuum manipulator's tip stiffness could be varied up to 3.61 times of the minimal value, demonstrating the effectiveness of the proposed stiffness variation approach.

Future works mainly include two aspects. First, a detailed mechanics modeling would be derived to reflect the stiffness accurately to achieve stiffness control. Second, the proposed idea would be applied to a practical design of a continuum surgical manipulator to further verify the concept's usefulness.

REFERENCES

[1] J. Burgner-Kahrs, D. C. Rucker, and H. Choset, "Continuum Robots for Medical Applications: A Survey," *IEEE Transactions on Robotics,* vol. 31, No.6, pp. 1261-1280, Dec 2015.

[2] W. McMahan, V. Chitrakaran, M. Csencsits, D. M. Dawson, I. D. Walker, B. A. Jones, M. Pritts, D. Dienno, M. Grissom, and C. D. Rahn, "Field Trials and Testing of the OctArm Continuum Manipulator," in *IEEE International Conference on Advanced Robotics (ICAR)*, Orlando, FL, USA, 2006, pp. 2336-2341.

[3] S. Liu, Z. Yang, Z. Zhu, L. Han, X. Zhu, and K. Xu, "Development of a Dexterous Continuum Manipulator for Exploration and Inspection in Confined Spaces," *Industrial Robot: An International Journal,* vol. 43, No.3, pp. 284-295, 2016.

[4] A. Pettersson, S. Davis, J. O. Gray, T. J. Dodd, and T. Ohlsson, "Design of a Magnetorheological Robot Gripper for Handling of Delicate Food Products with Varying Shapes," *Journal of Food Engineering,* vol. 98, No.3, pp. 332-338, June 2010.

[5] A. Sadeghi, L. Beccai, and B. Mazzolai, "Innovative Soft Robots Based on Electro-Rheological Fluids," in *IEEE/RSJ International Conference on Intelligent Robots and Systems (IROS)*, Vilamoura, Algarve, Portugal, 2012, pp. 4237-4242.

[6] M. J. Telleria, M. Hansen, D. Campbell, A. Servi, and M. L. Culpepper, "Modeling and Implementation of Solder-activated Joints for Single-Actuator, Centimeter-scale Robotic Mechanisms," in *IEEE International Conference on Robotics and Automation (ICRA)*, Anchorage, Alaska, USA, 2010, pp. 1681-1686.

[7] W. Shan, T. Lu, and C. Majidi, "Soft-matter Composites with Electrically Tunable Elastic Rigidity," *Smart Materials and Structures,* vol. 22, No.085005, pp. 1-8, July 2013.

[8] V. Saadat, R. C. Ewers, and E. G. Chen, "Shape Lockable Apparatus and Method for Advancing an Instrument through Unsupported Anatomy," US: USGI Medical, Inc., 2004.

[9] A. Degani, H. Choset, A. Wolf, and M. A. Zenati, "Highly Articulated Robotic Probe for Minimally Invasive Surgery," in *IEEE International Conference on Robotics and Automation (ICRA)*, Orlando, Florida, 2006, pp. 4167- 4172.

[10] Y.-J. Kim, S. Cheng, S. Kim, and K. Iagnemma, "A Stiffness-Adjustable Hyperredundant Manipulator Using a Variable Neutral-Line Mechanism for Minimally Invasive Surgery," *IEEE Transactions on Robotics,* vol. 30, No.2, pp. 382-395, April 2014.

[11] P. M. Loschak, S. F. Burke, E. Zumbro, A. R. Forelli, and R. D. Howe, "A Robotic System for Actively Stiffening Flexible Manipulators," in *IEEE/RSJ International Conference on Intelligent Robots and Systems (IROS)*, Hamburg, Germany, 2015, pp. 216-221.

[12] A. Shiva, A. Stilli, Y. Noh, A. Faragasso, I. De Falco, G. Gerboni, M. Cianchetti, A. Menciassi, K. Althoefer, and H. A. Wurdemann, "Tendon-Based Stiffening for a Pneumatically Actuated Soft Manipulator," *IEEE Robotics and Automation Letters,* vol. 1, No.2, pp. 632-637, July 2016.

[13] A. J. Loeve, O. S. v. d. Ven, J. G. Vogel, P. Breedveld, and J. Dankelman, "Vacuum Packed Particles as Flexible Endoscope Guides with Controllable Rigidity," *Granular Matter,* vol. 12, No.6, pp. 543-554, 2010.

[14] N. G. Cheng, M. B. Lobovsky, S. J. Keating, A. M. Setapen, K. I. Gero, A. E. Hosoi, and K. D. Iagnemma, "Design and Analysis of a Robust, Low-cost, Highly Articulated Manipulator Enabled by Jamming of Granular Media," in *IEEE International Conference on Robotics and Automation (ICRA)*, Saint Paul, Minnesota, USA, 2012, pp. 4328-4333.

[15] Y.-J. Kim, S. Cheng, S. Kim, and K. Iagnemma, "A Novel Layer Jamming Mechanism With Tunable Stiffness Capability for Minimally Invasive Surgery," *IEEE Transactions on Robotics,* vol. 29, No.4, pp. 1031-1042, Aug 2013.

[16] M. Langer, E. Amanov, and J. Burgner-Kahrs, "Stiffening Sheaths for Continuum Robots," *Soft Robotics,* vol. 5, No.3, pp. 291-303, Jun 2018.

[17] M. Mahvash and P. E. Dupont, "Stiffness Control of Surgical Continuum Manipulators," *IEEE Transactions on Robotics,* vol. 27, No.2, pp. 334-345, April 2011.

[18] K. Xu and N. Simaan, "An Investigation of the Intrinsic Force Sensing Capabilities of Continuum Robots," *IEEE Transactions on Robotics,* vol. 24, No.3, pp. 576-587, June 2008.

[19] A. Bajo and N. Simaan, "Hybrid Motion/Force Control of Multi-Backbone Continuum Robots," *International Journal of Robotics Research,* vol. OnlineFirst, pp. 1-13, 2015.

[20] K. Xu, M. Fu, and J. Zhao, "An Experimental Kinestatic Comparison between Continuum Manipulators with Structural Variations," in *IEEE International Conference on Robotics and Automation (ICRA)*, Hong Kong, China, 2014, pp. 3258-3264.

[21] B. Zhao, W. Zhang, Z. Zhang, X. Zhu, and K. Xu, "Continuum Manipulator with Redundant Backbones and Constrained Bending Curvature for Continuously Variable Stiffness," in *IEEE/RSJ International Conference on Intelligent Robots and Systems (IROS)*, Madrid, Spain, 2018, pp. 7492-7499.

[22] L. Wang, G. Del Giudice, and N. Simaan, "Simplified Kinematics of Continuum Robot Equilibrium Modulation via Moment Coupling Effects and Model Calibration," *ASME Journal of Mechanisms and Robotics,* vol. 11, No.5, pp. 051013-051013-12, 2019.

[23] R. J. Webster and B. A. Jones, "Design and Kinematic Modeling of Constant Curvature Continuum Robots: A Review " *International Journal of Robotics Research,* vol. 29, No.13, pp. 1661-1683, Nov 2010.

[24] P. Sears and P. E. Dupont, "Inverse Kinematics of Concentric Tube Steerable Needles," in *IEEE International Conference on Robotics and Automation (ICRA)*, Rome, Italy, 2007, pp. 1887-1892.

[25] T. Mahl, A. Hildebrandt, and O. Sawodny, "A Variable Curvature Continuum Kinematics for Kinematic Control of the Bionic Handling Assistant," *IEEE Transactions on Robotics,* vol. 30, No.4, pp. 935-949, Aug 2014.

[26] S. a. Zhang, Q. Li, H. Yang, J. Zhao, and K. Xu, "Configuration Transition Control of a Continuum Surgical Manipulator for Improved Kinematic Performance," *IEEE Robotics and Automation Letters,* vol. 4, No.4, pp. 3750-3757, Oct 2019.

[27] W. Zhang, Z. Yang, T. Dong, and K. Xu, "FABRIKc: An Efficient Iterative Inverse Kinematics Solver for Continuum Robots," in *IEEE/ASME International Conference on Advanced Intelligent Mechatronics (AIM)*, Auckland, New Zealand, 2018, pp. 346-352.

[28] S. Neppalli, M. A. Csencsits, B. A. Jones, and I. D. Walker, "Closed-Form Inverse Kinematics for Continuum Manipulators," *Advanced Robotics,* vol. 23, No.15, pp. 2077-2091, 2009.

[29] A. Garriga-Casanovas and F. Rodriguez y Baena, "Kinematics of Continuum Robots With Constant Curvature Bending and Extension Capabilities," *ASME Journal of Mechanisms and Robotics,* vol. 11, No.1, p. 011010, Feb 2019.

[30] K. Xu, J. Zhao, and M. Fu, "Development of the SJTU Unfoldable Robotic System (SURS) for Single Port Laparoscopy," *IEEE/ASME Transactions on Mechatronics,* vol. 20, No.5, pp. 2133-2145, Oct 2015.

[31] Z. Wu, Q. Li, J. Zhao, J. Gao, and K. Xu, "Design of a Modular Continuum-Articulated Laparoscopic Robotic Tool with Decoupled Kinematics," *IEEE Robotics and Automation Letters,* vol. 4, No.4, pp. 3545-3552, Oct 2019.

[32] K. Xu and N. Simaan, "Analytic Formulation for the Kinematics, Statics and Shape Restoration of Multibackbone Continuum Robots via Elliptic Integrals," *Journal of Mechanisms and Robotics,* vol. 2, No.011006, pp. 1-13, Feb 2010.